

NUMERICAL INVESTIGATION OF THE IRREGULAR BEHAVIOR OF HELICALLY COILED TUBE HEAT EXCHANGER CONCERNING PITCH CHANGES

by

Hessam MIRGOLBABA EI*

Department of Mechanical and Industrial Engineering,
University of Minnesota, Duluth, Minn., USA

Original scientific paper
<https://doi.org/10.2298/TSCI210621022M>

The convective heat transfer coefficient of the shell-side of helically coiled tube heat exchangers is numerically investigated in the present study. The present study's purpose is to evaluate the influence of geometrical parameters on local convective heat transfer coefficients. The heat exchangers' coil and shell-sides flow are fully laminar and steady. Grid independence for the numerical simulation is implemented, and the results are validated against corresponding experimental measurements. The highlights of the present simulation are the fluid-to-fluid model of the heat exchangers and the calculation of exact local heat transfer coefficients and its variation concerning pitch changes that are primarily prohibitive to conduct through experimental measurements on the same type of compact heat exchangers in terms of the complexity of the thermal energy exchange mechanisms. It is concluded from the results that the optimum pitch for the helically coiled tube that provides maximum heat transfer coefficients is achievable at some intermediate pitch values.

Keywords: *heat exchanger, helically coiled tube, thermal efficiency, heat transfer coefficients, convection*

Introduction

Helically coiled tube heat exchangers are among the most efficient compact heat exchangers. Their applications span a wide range of industries, such as pharmaceutical, heating, ventilating, and air-conditioning systems, and chemical, as primary thermal energy exchange devices such as boilers, evaporators, and refrigerating, to name a few [1-4]. The high performance and compactness of this type of thermal energy exchange device made it a focus of many research studies. The research studies ranged from experimental measurement, the primary method of evaluating such complicated geometries, to multiple forms of numerical investigations of these helically coiled tube heat exchangers. Different fluids and wide ranges of temperature changes in different fluid flow regimes have been the focus of studies in either natural, forced, or combined convection heat transfer forms. In most studies, particularly the ones conducted numerically, only simplified thermal boundary conditions on the coil surface were assumed. On the other hand, the author has undertaken a series of comprehensive numerical fluid-to-fluid simulations along with experimental verification [1, 2]. In those studies, for the first time, natural thermal boundary conditions were simulated by considering fluids at both sides of the coiled tubes, and wide ranges of mass flow rates were modeled to cover all possible thermal needs. An inclusive Nusselt number

* Author's e-mail: mirgolbabaei@gmail.com

calculation formula was proposed in those research studies and an appropriate expression for the unit's thermal efficiency [1, 2]. The numerical simulations reported in those studies were followed by detailed experimental measurements considering both laminar and turbulent fluid flow regimes. An inclusive expression was proposed for calculating the Nusselt number [3, 4]. The importance of understanding detailed features of helically coiled tube heat exchangers has motivated many researchers to focus on different aspects of similar types of compact heat exchangers. Maghrabie *et al.* [5] conducted an experimental study on the performance of a shell and helically coiled tube heat exchangers. They concluded that the thermal performance of their shell-and-tube heat exchanger was higher when the unit had a vertical orientation. Darzi *et al.* [6] carried out a study to investigate the thermal and hydrodynamic characteristics of the water flowing inside helically coiled tubes. Wang *et al.* [7] focused on a helically coiled-twisted trilobal tube and defined several indices to evaluate the flow characteristics inside the tube. Yong *et al.* [8] proposed formulations for optimizing the helically coiled tube. Abu-Hamdeh *et al.* [9] numerically investigated the thermal and hydraulic characteristics of a *sector-by-sector* helically coiled tube heat exchanger. They focused on turbulent flow inside the heat exchanger composed of the helically coiled tube-in-tube heat exchanger.

As can be perceived from the literature review, even in the most recent studies, the focus of the research studies has been on either the coiled-side heat transfer and hydraulic characteristics or the heat exchangers were composed of concentric coiled tubes rather than shell and tubes. Additionally, only some of the helically coiled tube heat exchangers reported in the literature are different from the compact type of heat exchanger that the author of the current study studied. The present study represents the in-detail analysis of the local convective heat transfer coefficient at the shell-side of helically coiled tube heat exchangers. The flow regime on both sides of the heat exchanger is assumed to be laminar under steady-state thermal and hydraulic conditions. Thermophysical properties of the fluids at both sides of the tube are evaluated as temperature functions. The varying thermophysical properties make the simulation of the thermal energy exchange more accurate. The numerical simulation is performed to calculate and analyze how the heat exchangers' geometrical characteristics affect the heat transfer coefficient along the height of the shell. Another novelty of the present study relies on the fact that it is, to the best of the author's knowledge, the only numerical simulation of this type of heat exchanger that evaluates the irregular behavior of the local heat transfer coefficient concerning dimensionless pitch variation.

Numerical algorithm

A steady-state condition of heat transfer between the hot fluid inside the helically coiled tube and fluid in the shell-side of helically coiled tube heat exchangers are numerically simulated in the present study. The governing equations are solved using CFD software. The CFD solver used in the present study is FLUENT. The SIMPLE-consistent (SIMPLEC) algorithm is adopted for pressure-velocity coupling [10]. The second-order upwind scheme is used to solve the momentum and energy governing equations. A relative convergence criterion of $1.0 \cdot 10^{-5}$ is adopted for the continuity equation and velocities in each direction. The convergence criterion for the energy conservation equation is set to $1.0 \cdot 10^{-8}$. The mass conservation equation (*i.e.*, continuity equation), momentum equation, and energy conservation equation, solved in this study are:

$$\frac{\partial}{\partial x_i}(\rho u_i) = 0 \quad (1)$$

$$\frac{\partial}{\partial x_i}(\rho u_i u_j) = -\frac{\partial P}{\partial x_i} + \frac{\partial}{\partial x_i} \left(\mu \frac{\partial u_j}{\partial x_i} \right) + \rho g_i \quad (2)$$

$$\frac{\partial}{\partial x_i}(\rho c_p u_i T) = \frac{\partial}{\partial x_i} \left(k \frac{\partial T}{\partial x_i} \right) \quad (3)$$

The thermophysical and transport properties of the fluid, both inside the tube and on the shell-side, are defined as functions of temperature only. The temperature dependencies of the properties are defined:

$$\rho(T) = -1.5629 \cdot 10^{-5} T^3 + 0.011778 T^2 - 3.0726 T + 1227.8 \quad (4)$$

$$c_p(T) = 1.1105 \cdot 10^{-5} T^3 - 0.0031078 T^2 - 1.478 T + 4631.9 \quad (5)$$

$$\mu(T) = -3.055 \cdot 10^{-8} T^3 + 1.6028 \cdot 10^{-5} T^2 - 0.0037524 T + 0.33151 \quad (6)$$

$$k(T) = 1.5362 \cdot 10^{-8} T^3 - 2.261 \cdot 10^{-5} T^2 + 0.010879 T - 1.0294 \quad (7)$$

In these correlations, the temperature is in Kelvin. Since the pressure of the fluids does not change appreciably, and since the pressure dependency of the properties of an incompressible fluid is negligible, temperature dependency is only considered in this study.

The pipe has an outer diameter d_{outer} . The coil has a diameter of D_{coil} (measured between the centers of the pipes), while the distance between two adjacent turns, called pitch, is noted as b . Coils were located inside the annular space between two coaxial cylindrical shells. Coil pitches of 1.5-2 tube diameters are studied. Constant temperature (80 °C) is considered for inlet flow to the coil-side and the inlet temperature of the shell-side fluid is 20 °C which is regarded as the same for all the models. Cold water enters the shell-side bottom (inlet mass-flow rate boundary condition) and leaves at the top (outlet boundary conditions). The shell-side mass-flow rates of water were in the range of 0.03-0.09 kg/s. These flow rates are like the flow rates in domestic SDHW applications. The fluid-flow in the shell-side is assumed to be laminar. To confirm this assumption, the cross-section area of the shell-side, which is available for flow pass, has been determined, and the Reynolds number according to this section has been calculated, supposing the flow to be perpendicular to this section. This cross-section is shown in fig. 1. This figure demonstrates the flow passage cross-section inside the space confined by the inner and outer shells and helical tubes. The shaded area is the net area through which the fluid moves upward inside the shell-side of the heat exchanger. It was found that the Reynolds number for the flow perpendicular to this surface, based on the equivalent diameter of this cross-section, is small enough that the laminar regime assumption is valid.

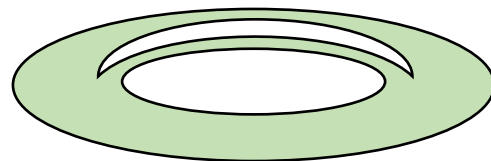


Figure 1. The shaded area represents a cross-section area of the shell-side of the heat exchanger that is available for flow

Hot water enters the helical coil at the top (mass-flow inlet boundary condition) and leaves at the bottom (outflow boundary condition). The coil-side water mass-flow rate is 0.03 kg/s. Also, heat conduction through the tube wall of 0.86 mm thickness is modeled. The overall flow configuration in the exchanger is countercurrent. Several studies have identified that a complex flow pattern exists inside a helical pipe, resulting in an enhancement in heat transfer [11]. The curvature of the coil governs the magnitude of the centrifugal force, while

the pitch (or helix angle) influences the torsion which the fluid is subjected. The centrifugal force results in the development of secondary flow [11]. Owing to this curvature effect, the fluid streams on the outer side of the pipe move faster than the fluid streams on the inner side of the tube. The difference in velocity sets secondary flows, which pattern changes with the Dean number of the flow, De . According to the study conducted by Schmidt [12], the critical Reynolds number for the helical pipe flow, which determines the flow regime, is related to the curvature ratio:

$$Re_{Cr} = 2100 \left[1 + 12 \left(\frac{d_{outer}}{D_{coil}} \right)^{1/2} \right] \quad (8)$$

The coil side water flow regime is laminar according to the mass-flow range. Also, the material of the coil tube is copper. Seven different coils have been considered for the same shape and dimension of the shell part of the heat exchanger, and seven different coils have been considered. Dimensions of the heat exchangers modeled are presented in tab. 1. Various boundary conditions for each coil are simulated by changing the heat exchanger model's mass-flow rate on the shell-side. In total, 28 simulations have been conducted.

Table 1. Coils and shell specifications

D_{oc} [mm]	D_{ic} [mm]	d_{outer} [mm]	t [mm]	D_{coil} [mm]	b [mm]	N	H [mm]	A_{coll} [m ²]
160	90	9.52	0.86	125	14.3	24	360	0.282
160	90	9.52	0.86	125	16.2	21	360	0.247
160	90	9.52	0.86	125	17.1	20	360	0.236
160	90	9.52	0.86	125	19	18	360	0.213
160	90	12.5	0.86	125	21.3	16	360	0.249
160	90	12.5	0.86	125	22.5	15	360	0.234
160	90	12.5	0.86	125	25	13	360	0.203

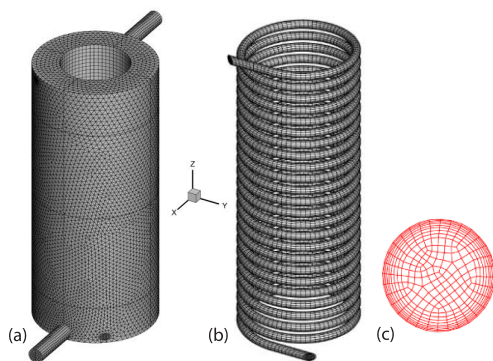


Figure 2. A representative example of the mesh types used for the numerical simulation; (a) at the outer surface of the shell, (b) at the surface of one the coil located in the annular space in between the inner and outer shell, and (c) at the cross-section of the coil inside

Grid independence analysis

A graphical representation of one of the final grids used for one of the specifications mentioned in tab. 1 is demonstrated in fig. 2. Structured grids were used to mesh the pipe fluid volume. A boundary-layer mesh was generated for the pipe fluid volume. Due to the highly irregular shell-side flow passage, an unstructured grid was developed in that part of the model. Also, since for the models with small coil pitch, it was hardly possible, and mostly impossible, to generate a very dense grid on the shell-side, another criterion has been considered as a limitation in the mesh generation procedure. For the shell-side of the models, first, the outer surface of the coils, the shell's inner cylinder, and the shell's outer cylinder are meshed.

Then the mesh is generated for the entire space of the shell-side. The maximum and minimum mesh density for shell-side fluid among all the models are $8.30 \cdot 10^7 \text{ cell/m}^3$, $4.64 \cdot 10^7 \text{ cell/m}^3$, respectively. Grid independence analysis was carried out before performing a complete set of simulations. To perform the grid independence analysis, specific numbers of cells are generated on the inner and outer shell walls and the outer surface of the coil. Then, the space in between them was meshed. Then the numerical simulation is performed, and the data analysis is performed. At the second step of the grid independence analysis, the number of cells at the inner and outer cylinder and outer coil surface is doubled, and similar calculations on the data are performed. Then, the results from both sets of measures are compared. This comparison has been conducted for coil No. 7, and the results for the local convection heat transfer coefficients are reported in the previous studies by the author [1, 2]. The maximum discrepancy between the results is less than 0.7%. It proves that the initial number of cells generated at the surface of the coils, at the inner and outer cylinder as well, provides a good resolution. Still, the finer grid is used for the simulation.

Numerical model validation

The accuracy of the numerical simulation is verified against experimental measurements, and the validity has been reported in the primary part of the study in [1, 2]. For clarity, the validation is reproduced here in Figure 3. The experimental measurements were for a heat exchanger with coil pitch, inner cylinder diameter, outer cylinder diameter, heat exchanger height, and several coil pitch of 16.47 mm, 88.9 mm, 157 mm and 383 mm and 23.25, respectively [3, 4]. The coil was formed carefully using a 9.52 OD straight copper tube. To be consistent with the experimental geometry, the models with the coil No. 2 are chosen for verification. As can be seen, for the same range of heat flux, relatively close values for the average heat transfer coefficient are obtained. The experimental measurement was under either laminar, turbulent, or mixed fluid motion inside the shell-side. As a result, the experimental measurements have covered the heat transfer coefficient's upper range, as turbulence's effect was present. The resulting figure is demonstrated to validate the numerical values with the closest experimental measurement conditions while keeping the average heat flux as the common point between the measured and simulated data. Additionally, while in the numerical analysis, the flow inside the helical coil is set up to be completely laminar, in the experimental set-up, there was no guarantee that the flow inside the tube would be completely laminar at all points. The minor discrepancy in fig. 3 can be attributed to this difference between the fluid-flow regimes inside the tube.

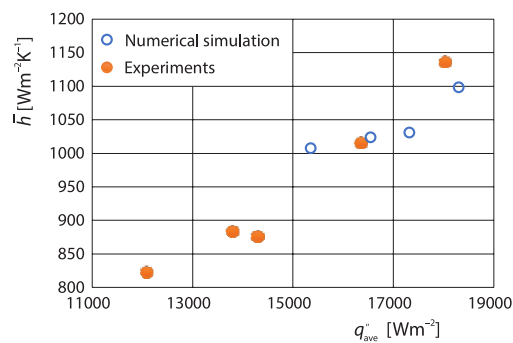


Figure 3. Comparison of the numerical simulation results with the experimental measurement reported in [3, 4]; the figure is from [1, 2]

Results and discussion

Heat transfer coefficient

The current study focuses on the thermal behavior of the heat exchanger's shell-side. While the average heat transfer coefficient of the heat exchanger may be calculated from the equation:

$$q = \dot{m}_C c_p (T_{C,o} - T_{C,i}) \quad (9)$$

$$h_{ave} = \frac{q}{(T_{C,ave} - T_{S,ave})} \quad (10)$$

where $T_{C,ave}$ and $T_{S,ave}$ are the average temperature of the helical coil surface (inside the shell) and the average shell-side temperature, respectively. The corresponding local convective heat transfer coefficient depends on the local temperature gradient along the shell and temperature gradient along the helical tube on the shell-side surface of the coil. The proposed heat exchanger aims to be as compact as possible to provide an efficient heat transfer mechanism between two streams inside the shell and the coil. The pitch of the helical coil is a factor in defining the heat exchanger's compactness for each selected tube diameter. To that end, it is critical to evaluate and compare the rate of thermal energy exchange on the shell-side for a range of pitch values to find the optimum pitch. Figures 4-7 demonstrate the shell-side convection heat transfer coefficient shell-side mass-flow rates of 0.03 kg/s, 0.04 kg/s, 0.05 kg/s and 0.09 kg/s, respectively, for a tube diameter of 9.52 mm. These diagrams are for models No. 1-4, corresponding to the dimensionless coil pitch of 1.5, 1.7, 1.8, and 2, respectively. This figure's shells 0.03 kg/s. The coil-side mass-flow rate is the same for all cases. While the increase of the coil pitch will initially decrease heat transfer, as the dimensionless coil pitch changes from 1.5-1.8, further growth leads to significant growth in the heat transfer coefficient. Similar behavior of the heat transfer coefficient concerning coil pitch diameter has been reported in a study focusing on natural-convection on the shell-side of the heat exchanger. The trend of the heat transfer coefficient change concerning dimensionless pitch could be attributed to the development of the thermal boundary-layer and thickness along the height of the heat exchanger and the helical direction of the coil. That will be discussed separately in the next section.

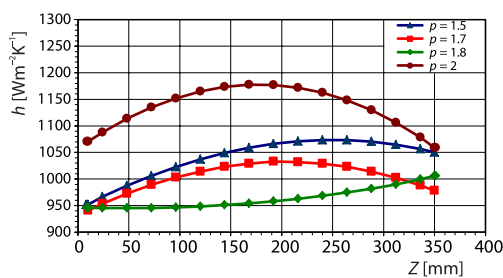


Figure 4. Local convection heat transfer coefficient vs. the direction along the vertical orientation of the unit, z , for the shell-side mass-flow rate of 0.03 kg/s for different coil dimensionless coil pitch for tube diameter 9.52 mm

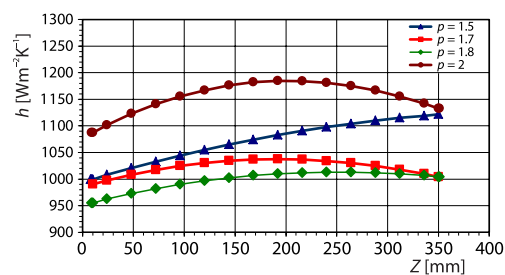


Figure 5. Local convection heat transfer coefficient vs. the direction along the vertical orientation of the unit, z , for the shell-side mass-flow rate of 0.04 kg/s for different coil dimensionless coil pitch for tube diameter 9.52 mm

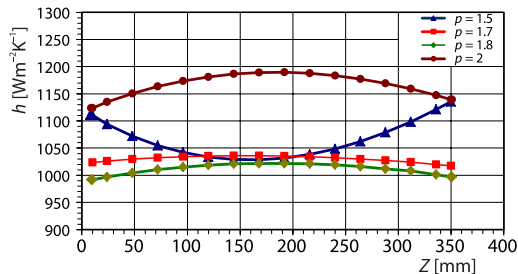


Figure 6. Local convection heat transfer coefficient vs. the direction along the vertical orientation of the unit, z , for the shell-side mass-flow rate of 0.05 kg/s for different coil dimensionless coil pitch for tube diameter 9.52 mm

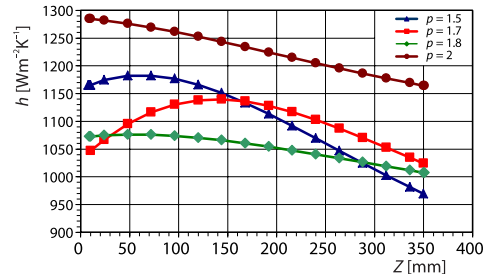


Figure 7. Local convection heat transfer coefficient vs. the direction along the vertical orientation of the unit, z , for the shell-side mass-flow rate of 0.09 kg/s for different coil dimensionless coil pitch for tube diameter 9.52 mm

Figures 8-11 demonstrate the shell-side convection heat transfer coefficient shell-side mass-flow rates of 0.03 kg/s, 0.04 kg/s, 0.05 kg/s, and 0.09 kg/s, respectively, for a tube diameter of 12.5 mm. These diagrams are for models No. 5-7, corresponding to the dimensionless coil pitch of 1.7, 1.8, and 2, respectively. This figure's shell-side mass-flow rate is 0.03 m/s. For this larger tube diameter, 12.5 mm, the changing trend of the convection heat transfer coefficient is quantitatively following that of the 9.52 mm tube diameter. It is noteworthy that the dimensionless pitch of 1.5 is not part of the results in these diagrams. The reason for not demonstrating the results for the dimensionless pitch of 1.5 is that the numerical simulation did not represent a reliable trend. It was inspected to need further modelling and grid rearrangement. Similarly to what is observed for the lower diameter, the increment of the dimensionless pitch of the coil initially leads to a decrease in the local heat transfer coefficient followed by a significant increase in the heat transfer coefficient. For this tube diameter, the escalation of the heat transfer coefficient may not be relatively as substantial as that was observed for the lower tube diameter, *i.e.*, it may not increase that much to be larger than the heat transfer coefficient of the coil with dimensionless pitch 1.7, at all points along the heat exchanger. It is noteworthy that, for both tube diameters, the behavior of helical coil, as had been reported by other authors with a limited number of dimensionless pitches, is consistent with what was reported in this article. While there has not been a thorough explanation of this behavior in other experimental works, this present study has tried to provide a more comprehensive and exhaustive explanation, given the nature of a numerical simulation. The change in the behavior of the heat transfer coefficient concerning the dimensionless pitch has been the focus of the current study. Although the shape of the curve for a specific pitch in that figure is different from those of the other dimensionless pitches, it is adjusted by looking at the temperature contours in the shell-side of the heat exchanger for that specific pitch. While irregular behavior of helically coiled tubes concerning the change of the dimensionless pitch has been reported in some experimental works, this work is among the pioneer ones (if not the first one) that demonstrates the local heat transfer profiles along the coils. The grid generation in the shell-side of this type of heat exchanger imposed a significant limitation as to which degree the dimensionless pitch could be decreased. This latter issue prohibited further decreases of the space between successive coil pitches for both tube diameters but more significantly for the larger tube diameter. This limitation is subject to further investigation in the future study of this type of heat exchanger.

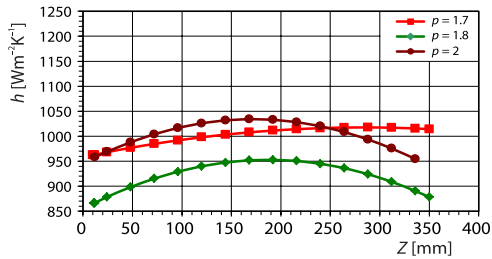


Figure 8. Local convection heat transfer coefficient vs. the direction along the vertical orientation of the unit, z , for the shell-side mass-flow rate of 0.03 kg/s for different coil dimensionless coil pitch for tube diameter 12.5 mm

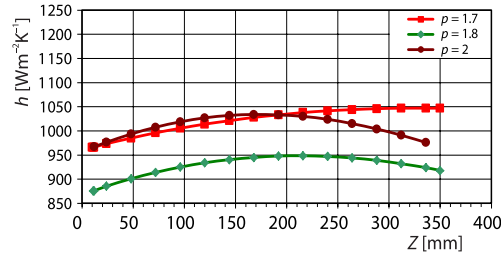


Figure 9. Local convection heat transfer coefficient vs. the direction along the vertical orientation of the unit, z , for the shell-side mass-flow rate of 0.04 kg/s for different coil dimensionless coil pitch for tube diameter 12.5 mm

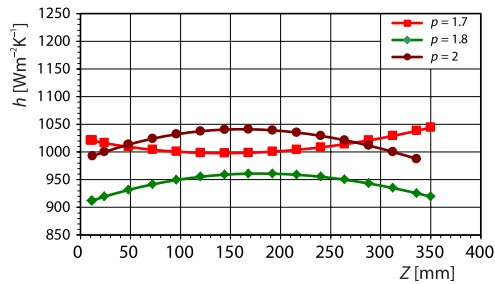


Figure 10. Local convection heat transfer coefficient vs. the direction along the vertical orientation of the unit, z , for the shell-side mass-flow rate of 0.05 kg/s for different coil dimensionless coil pitch for tube diameter 12.5 mm

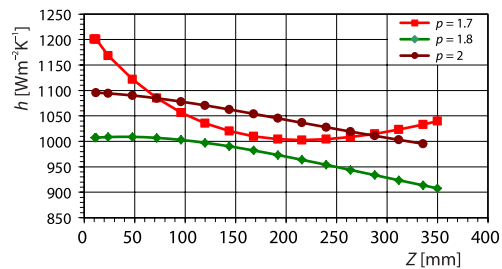


Figure 11. Local convection heat transfer coefficient vs. the direction along the vertical orientation of the unit, z , for the shell-side mass-flow rate of 0.09 kg/s for different coil dimensionless coil pitch for tube diameter 12.5 mm

Temperature distribution

The heat transfer coefficient variation on the shell-side of the heat exchanger may be well explained by exploring the temperature distribution inside the shell and on the coil surface. The temperature distribution is a revealing factor in justifying the heat transfer mechanism trend along the vertical length of the shell. The figures in this section demonstrate the temperature values on the shell-side of the heat exchanger based on the entire computational cells on that side. The temperature values in absolute scale are plotted for all computational nodes inside the shell-side fluid, and the computational nodes at the coil surface at the shell-side of the heat exchanger, in figs. 12(a) and 12(b), respectively. There are two significant areas in the scattered temperature plot of the shell-side fluid temperature. The upper area in that plot, fig. 12(a), precisely coincides with the temperature distribution plotted in fig. 12(b). The heat transfer rate and, consequently, the convection heat transfer coefficient are a function of the temperature difference between these two significant clusters of points in fig. 12(a). The convection heat transfer coefficient is also related to the fluid's flow velocity and thermophysical properties. The higher the dimensionless pitch for the same tube diameter, the lower the fluid bulk motion is on the shell-side, given the more significant volume present for the passage of the shell-side fluid. Inspecting the temperature distribution in the shell-side of the heat exchanger and the coil surface at the shell-side, for other models, demonstrates the temperature gradient at the

boundary-layer of the shell-side fluid to be first decreasing then increasing again, as the dimensionless pitch increases, for the tube diameter 9.52 mm. The decrease of the average velocity on the shell-side, accompanied by the decrement in the temperature gradient of the shell, results in the decline of the corresponding heat transfer coefficient value. However, as the temperature gradient increases, by further increasing the dimensionless pitch, although the velocity of the shell-side fluid-flow decreases, the effect of increased temperature distribution sounds dominates the velocity decrease. Similar behavior is observed for the large tube diameter, 12 mm.

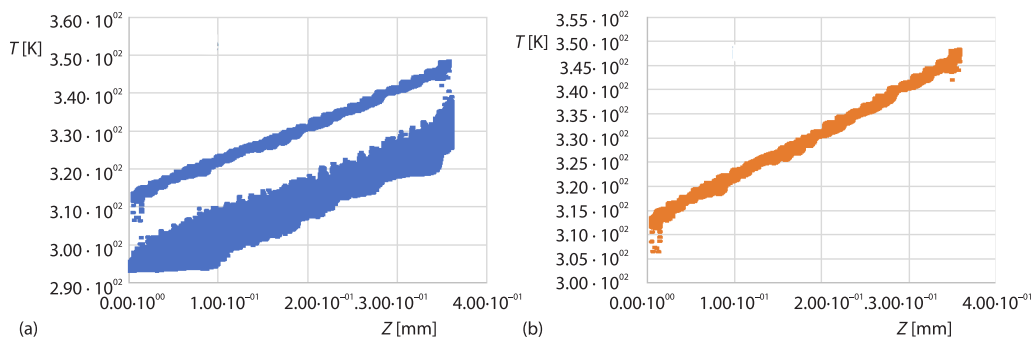


Figure 12. Temperature values at computational nodes for the fluid at (a) the shell-side of the heat exchanger and (b) coil surface at the shell-side, for geometry No. 1, for the shell-side mass-flow rate of 0.03 kg/s

To better demonstrate the temperature distribution around the coil surface on the shell-side, the temperature contour for different values of dimensionless pitches is plotted in fig. 13. As can be seen, although the temperature gradient increases, from configuration No. 1, figs. 13(a) and 13(b) to configuration No. 2, figs. 13(c) and 13(d), as the number of coils inevitably increases, as well, the Reynolds number slightly decreases thus the average velocity of the fluid particles. A decrease in the velocity will adversely affect the convection heat transfer coefficients. The effect of the reduced average velocity dominates that of the increased temperature gradients on the coil surface in the shell-side, and overall, the corresponding heat transfer coefficient decreases. The reduced cross-sectional average velocity also leads to lower density as the shell-side fluid-flow residence time increases. These effects combined contribute towards an even lower Reynolds number. The boundary-layer thickness further increases from configuration No. 2, figs. 13(c) and 13(d), to configuration No. 3, figs. 13(e) and 13(f), whereas the temperature gradient does not competitively increase. Combined with the former phenomena, the latter effect results in a reduced heat transfer coefficient. Additionally, as already mentioned, the increased dimensionless pitch in configuration No. 3 means a smaller number of coils and thus reduced average bulk motion of the shell-side flow than those of No. 2. These three effects combined result in even further convection heat transfer coefficient depreciation. The change of temperature contours from geometry No. 3 to geometry No. 4 demonstrates an utterly different trend than the ones observed for No. 1 to No. 2, and No. 2 to No. 3. Although the number of coils. Thus, the average bulk cross-sectional motion of the shell-side flow is smaller than the first three geometries already discussed. The increased space between the coil turns contributes towards a higher temperature gradient with less boundary-layer thickness. This trend for temperature contours and the corresponding boundary-layers increases the convection heat transfer coefficient for a dimensionless pitch value of 2.

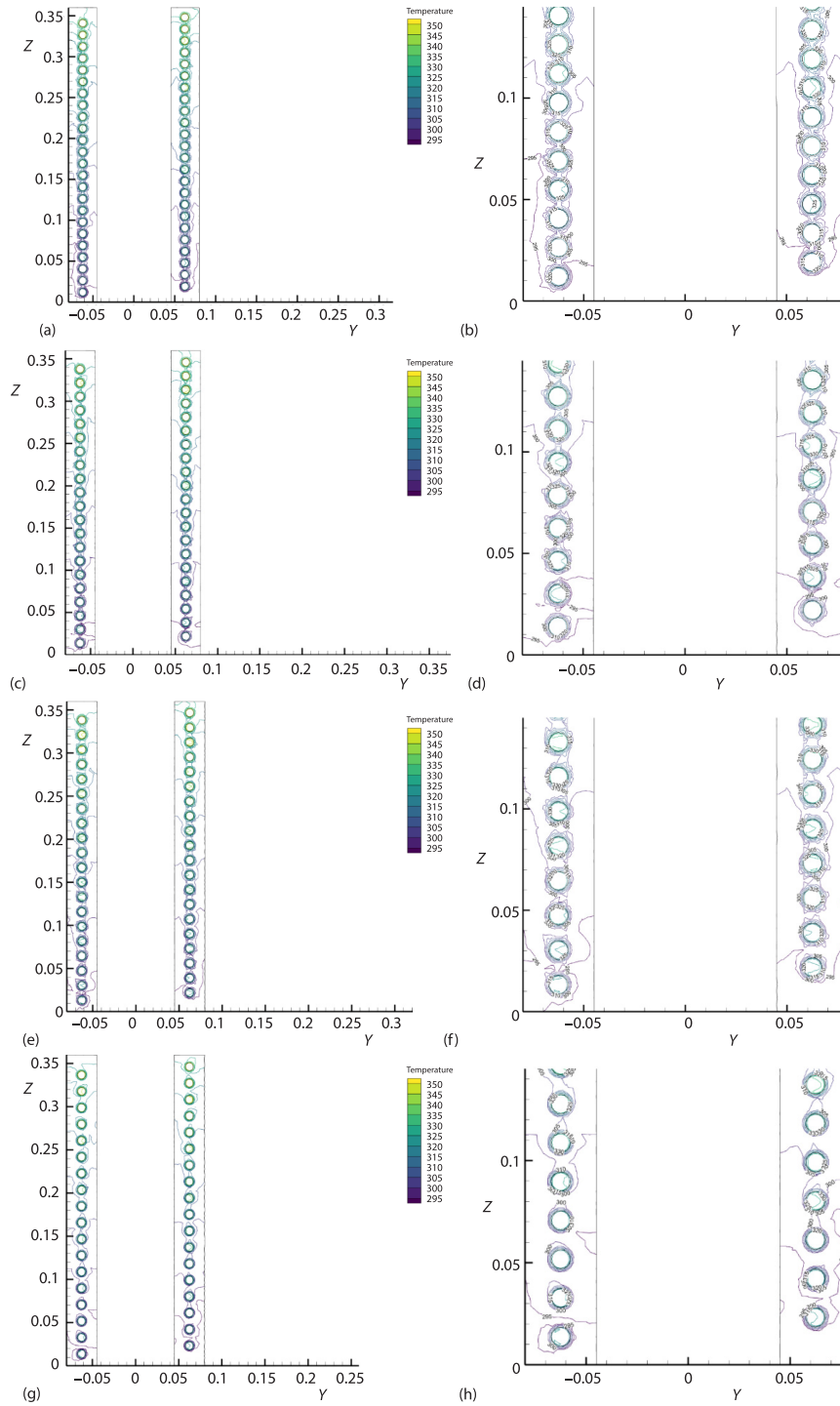


Figure 13. Temperature contour lines for configurations; (a) and (b) No. 1, (c) and (d) No. 2, (e) and (f) No. 3, and (g) and (h) No. 4, with mass-flow rate of 0.03 kg/m^3 at the shell-side

Figure 14 demonstrates the temperature contours of the heat exchanger geometries for the models with the same shell-side mass-flow rate but different dimensionless pitch values. The temperature contours for the larger tube diameter, 12.5 mm, demonstrate similar conditions to that of the lower tube diameter, 9.52 mm, as the dimensionless pitch of the coil increases. The boundary-layer thickness significantly increases as the dimensionless coil pitch increases from 1.7-1.8, whereas the average cross-sectional bulk motion decreases. This phenomenon

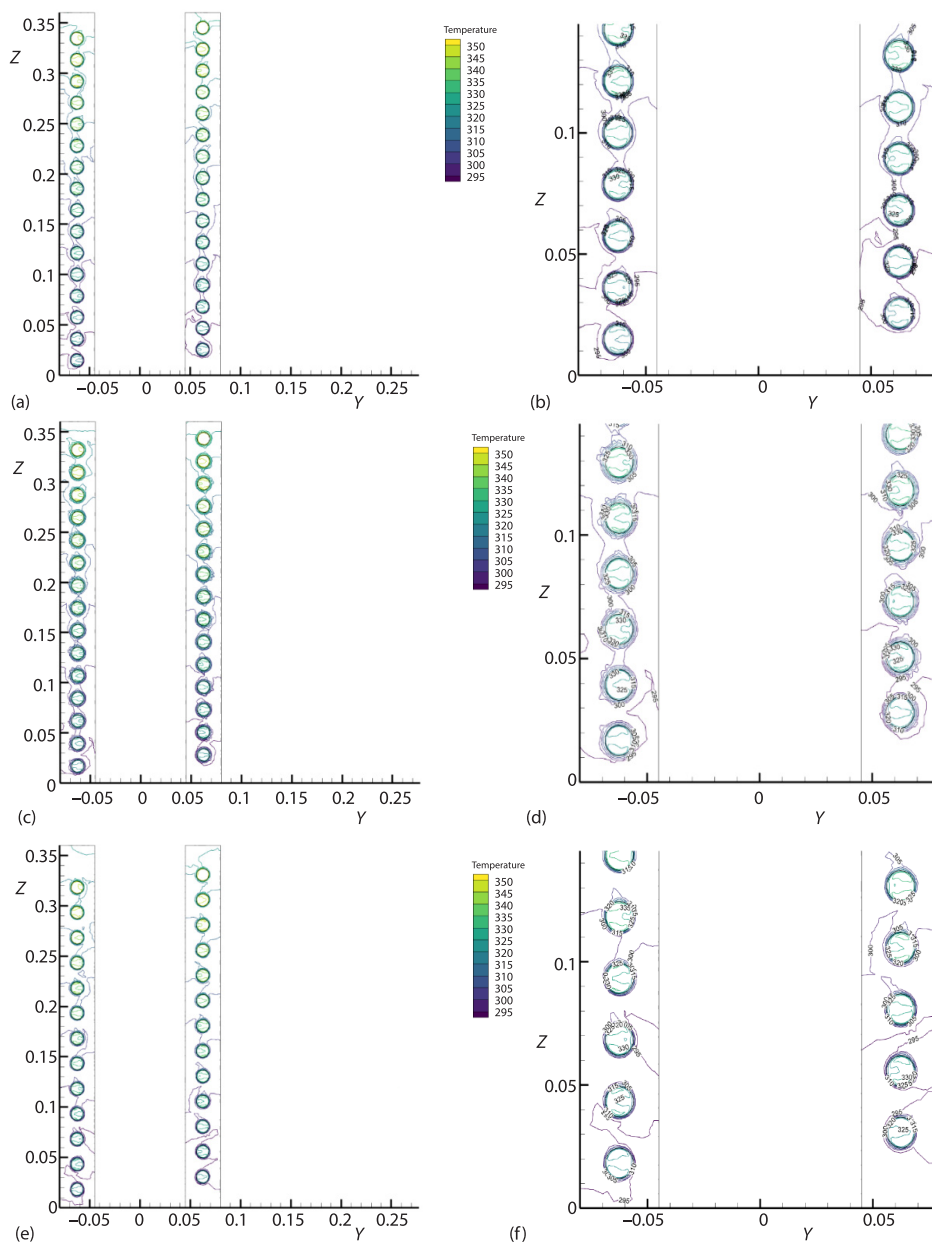


Figure 14. Temperature contour lines for configurations; (a) and (b) No. 5, (c) and (d) No. 6, and (e) and (f) No. 7, with mass-flow rate of 0.03 kg/m³ at the shell-side

led to reduced local heat transfer coefficients. Further increase in coil dimensionless pitch – 1.8 to 2, results in, once again, having a thinner boundary-layer and higher temperature gradient on the coil surface. While the cross-sectional bulk motion would decrease because of having a smaller number of coils, thus a larger cross-sectional area on the shell-side is outweighed by the thinner boundary-layer and more significant temperature gradient. As a result, the local heat transfer coefficient increases. However, this increase is insufficient to have the local coefficient magnitudes pass beyond that of the lowest dimensionless pitch. Higher pitch values lead to some possible dead zones and allow for more of a circular boundary-layer development around the coil surface at the shell-side.

Conclusion

Constructing a heat exchanger in a more compact form is typically desirable, based on getting more contact area while keeping the total volume constant. However, as demonstrated in this novel study, only sometimes those factors combined result in higher heat transfer rate and or local heat transfer coefficients at both or either side of helically coiled tube heat exchangers. The present study was directed toward examining the effect of the compactness level of the coiled tube heat exchanger on the local heat transfer coefficients. The unique geometry of the helically coiled tube heat exchanger presented in the present study is the first to be studied in detail. It offers novel compactness in terms of the area-to-volume ratio. The double cylinder structure of the unit strongly contributes towards getting a higher contact area between the fluid in the shell-side and the hot surface of the coiled tube holding the hot fluid-flow inside. The present study's main novelty lies in analyzing the effect of the dimensionless pitch on the local heat transfer coefficient of the shell-side. It has been demonstrated that increasing the dimensionless pitch for different tube diameters does not necessarily result in decreased heat transfer coefficient. Although the bulk motion of the shell-side fluid-flow decreases as the dimensionless pitch increases, the heat transfer coefficient decreases and then increases. While, for the small tube diameter, the growth of the dimensionless pitch eventually results in increased convection heat transfer rate coefficient, even more than the lowest pitch considered, that increase may not be to the level that could pass beyond the heat transfer coefficient for the lowest dimensionless pitch values, at all points along the height of the unit for the higher tube diameter. This latter phenomenon may imply that either lower or higher than the dimensionless pitch of 2 could cause a significantly higher heat transfer coefficient. Figuring out the best boundary-layer form and its development along the coil can lead to optimum coil pitch, which is necessary to determine the optimum helically coiled tube heat exchanger.

Nomenclature

A	– area, [m ²]	q	– heat transfer rate, [W]
b	– dimensional coil pitch, [m]	q''	– heat flux, [Wm ⁻²]
c_p	– specific heat, [Jkg ⁻¹ K ⁻¹]	Re	– Reynold number ($= \rho u D / \mu$)
D	– diameter, [m]	T	– temperature, [°C or K]
d	– diameter, [m]	t	– thickness, [m]
g	– i^{th} component of the gravitational acceleration, [ms ⁻²]	u	– velocity component, [ms ⁻¹]
H	– height, [m]	x	– co-ordinate axis, [m]
h	– convection heat transfer coefficient, [Wm ⁻² K ⁻¹]	Z	– vertical co-ordinate along the height of the heat exchanger, [m]
\bar{h}	– average heat transfer coefficient, [Wm ⁻² K ⁻¹]	$\partial/\partial x_i$	– partial derivative with respect to x_i
k	– thermal conductivity, [Wm ⁻¹ K ⁻¹]		
N	– number of coil pitches		
p	– pressure, [Nm ⁻²]	<i>Greek symbols</i>	
		μ	– dynamic viscosity, [kgm ⁻¹ s ⁻¹]

ρ – density, [kgm⁻²]

Subscripts

ave – average value of the
corresponding quantity
Cr – critical value

coil – coil
 i – i^{th} component
ic – inner cylinder
oc – outer cylinder
outer – outer dimension

References

- [1] Mirgolbabaei, H., *et al.*, Numerical Estimation of Mixed Convection Heat Transfer in Vertical Helically Coiled Tube Heat Exchangers, *International Journal for Numerical Methods in Fluids*, 66 (2011), 7, pp. 805-819
- [2] Mirgolbabaei, H., Numerical Investigation of Vertical Helically Coiled Tube Heat Exchangers Thermal Performance, *Applied Thermal Engineering*, 136 (2018), May, pp. 252-259
- [3] Ghorbani, N., *et al.*, Experimental Study of Mixed Convection Heat Transfer in Vertical Helically Coiled Tube Heat Exchangers, *Experimental Thermal and Fluid Science*, 34 (2010), 7, pp. 900-905
- [4] Ghorbani, N., *et al.*, An Experimental Study of Thermal Performance of Shell-and-Coil Heat Exchangers, *International Communications in Heat and Mass Transfer*, 37 (2010), 7, pp. 775-781
- [5] Maghrabie, H. M., *et al.*, Performance of a Shell and Helically Coiled Tube Heat Exchanger with Variable Inclination Angle: Experimental Study and Sensitivity Analysis, *International Journal of Thermal Sciences*, 164 (2021), June, 106869
- [6] Darzi, A. A. R., *et al.*, Numerical Investigation on Thermal Performance of Coiled Tube with Helical Corrugated Wall, *International Journal of Thermal Sciences*, 161 (2021), Mar., 106759
- [7] Wang, G., *et al.*, Experimental and Numerical Investigation on Hydraulic and Thermal Performance in the Tube-Side of Helically Coiled-Twisted Trilobal Tube Heat Exchanger, *International Journal of Thermal Sciences*, 153 (2020), July, 106328
- [8] Yong, H., *et al.*, Multi-Objective Optimization of Helically Coiled Tube Heat Exchanger Based on Entropy Generation Theory, *International Journal of Thermal Sciences*, 147 (2020), Jan., 106568
- [9] Abu-Hamdeh, N. H., *et al.*, Analysis of the Thermal and Hydraulic Performance of the Sector-by-Sector Helically Coiled Tube Heat Exchangers as a New Type of Heat Exchangers, *International Journal of Thermal Sciences*, 150 (2020), Apr., 106229
- [10] Versteeg, H. K., Malalasekera, W., *An Introduction Computational Fluid Dynamics: The Finite Volume Method*, Lognman Scientific & Technical, Harlow, UK, 1995
- [11] Dravid, A. N., *et al.*, Effect of Secondary Fluid Motion on Laminar-Flow Heat Transfer in Helically-Coiled Tubes, *AIChE Journal*, 17 (1971), 5, pp. 1114-1122
- [12] Schmidt, E. F., Wärmeübergang und Druckverlust in Rohrschlangen (in German), *Chemie Ingenieur Technik*, 39 (1967), 13, pp. 781-789